SLAC-PUB-12237

March 2007

SIMULATIONS OF THE ELECTRON CLOUD BUILD UP AND INSTABILITIES FOR VARIOUS ILC DAMPING RING CONFIGURATIONS[a]

Mauro Pivi[b], Tor O. Raubenheimer, Lanfa Wang

SLAC, Menlo Park, California 94025, USA

Kazuhito Ohmi

KEK, Tsukuba, Japan

Rainer Wanzenberg

DESY, Hamburg, Germany

Andrzej Wolski

University of Liverpool and the Cockcroft Institute, UK

Frank Zimmermann

CERN, 1211 Geneva 23, Switzerland

---

[a] Work supported by the Director, Office of Science, High Energy Physics, U.S. DOE under Contract No. DE-AC02-76SF00515 and the Commission of the European Communities Contract No. RIDS-011899

[b] mpivi@slac.stanford.edu

Submitted to Physical Review Special Topics Accelerator And Beams

Abstract

In the beam pipe of the positron damping ring of the International Linear Collider (ILC), an electron cloud may be first produced by photoelectrons and ionization of residual gases and then increased by the secondary emission process[1].

This paper reports the assessment of electron cloud effects in a number of configuration options for the ILC baseline configuration. Careful estimates were made of the secondary electron yield (sometimes in the literature also referred as *secondary emission yield* SEY or δ, with a peak value δ_{max}) threshold for electron cloud build-up, and the related single- and coupled-bunch instabilities, as a function of beam current and surface properties for a variety of optics designs. When the configuration for the ILC damping rings was chosen at the end of 2005, the results from these studies were important considerations. On the basis of the joint theoretical and experimental work, the baseline configuration currently specifies a pair of 6 km damping rings for the positron beam, to mitigate the effects of the electron cloud that could present difficulties in a single 6 km ring. However, since mitigation techniques are now estimated to be sufficiently mature, a reduced single 6-km circumference is presently under consideration so as to reduce costs.

PACS Numbers: 29.20.Dh, 29.27.Bd, 41.75.Lx, 52.35.–g, 79.20.Hx

Introduction

The TESLA TDR specified a “dog-bone” damping ring with 17 km circumference. The ILC collaboration invested considerable effort studying alternative damping ring configurations in order to reduce the circumference, increase the dynamic aperture, and

reduce space charge effects. However, the build-up of the electron cloud is strongly dependent on the bunch separation, which decreases with the damping ring circumference. Reduction in the circumference could make electron cloud effects more severe. Coupling between electrons in the cloud and the circulating beam can cause coupled-bunch instabilities, coherent single-bunch instabilities or incoherent tune spreads that may lead to increased emittance, beam blow-up and ultimately to beam losses [1] [2] [3] [4] [5] [6] [7] [8] [9] [10] [11]. All these effects would directly affect the collider luminosity, and therefore it is important to suppress the electron cloud in the positron damping ring. In this paper, we summarize the simulation results for the electron cloud build-up and the related single-bunch instabilities. These results were obtained by an international collaborative effort[12] studying eight different damping ring lattice designs, including the original TESLA design. The main parameters of these lattices are listed in Table 1, 2 and 3. The nomenclature (PPA, OTW etc.) is designed to provide a means of referring to the lattices that is objective, and not colored by any associations.

SIMULATION CAMPAIGN

The electron cloud effects are prominent among the criteria to be considered when choosing the damping ring circumference and setting the specifications for the vacuum system. To provide operational flexibility, the damping rings should also be capable of accommodating a range of bunch charges; to provide a given luminosity, reducing the bunch charge means increasing the number of bunches, and decreasing the bunch separation.

Damping rings with circumferences significantly below 6 km would require performance specifications on the injection and extraction kickers that are presently considered too

demanding. We therefore focused our studies on rings with circumferences of 6 km and larger.

As far as possible, the different reference lattices were analyzed with the same techniques and assumptions applied to each. The methodology was as follows:

- Pertinent parameters were compiled, including beam sizes in arcs, wiggler, and straights, bunch spacing, tunes, beta functions, chamber dimensions, and lengths of regions with magnetic fields.
- Electron cloud build-up was simulated for the different regions (arcs, wigglers, straights) in the rings, considering actual sets of beam parameters and for two different secondary emission yields.
- Common secondary emission yield [13] [14] models [2] [12] [15] [16] were used for benchmarking the simulation codes. Predictions of electron cloud build-up in the damping rings using different simulation codes were compared.
- For simulations in the wigglers, the field was modeled at various levels of sophistication, and the importance of refined models was explored.
- Single-bunch wake fields and the thresholds of the fast head-tail TMCI-like instability were estimated both by simulations and analytically.
- Multi-bunch wake fields and growth rates were inferred from build-up and multi-bunch simulation codes.
- Tune shifts induced by the electron cloud were calculated and compared.

Codes used for simulations of the build-up of electron cloud in these studies [17] [18] were POSINST (M. Furman LBNL and M. Pivi SLAC), ECLOUD (F. Zimmermann et al. CERN) and CLOUDLAND (L. Wang SLAC). Instability simulation codes used were

PEHTS (K. Ohmi KEK) and HEAD-TAIL (G. Rumolo and F. Zimmermann CERN) for single-bunch instabilities[19 20], and PEI-M (K. Ohmi KEK) for multi-bunch instabilities. In this paper, we use the notation I, II, III, IV, V and VI to refer to the respective simulation codes described above.

As part of these studies, we performed simulations for the PEP-II and KEKB positron rings with parameters given in Table 4, and compared the electron cloud build-up and instability characteristics with the different DR configuration options. Studies to benchmark the simulation codes against experimental data are ongoing at the CERN SPS, DAΦNE, LANL PSR, PEP-II and KEKB; so far, the results of the simulation codes are generally consistent with the experimental data assuming certain surface properties.

SINGLE-BUNCH INSTABILITY

The strength of the single-bunch instability due to electron cloud is assumed to be determined by the average electron density along the ring,

$$\langle \rho_e \rangle = \frac{1}{C} \oint \rho_e(s) ds \qquad (1)$$

where C and ρ_e are the ring circumference and the electron density at ring locations, respectively. The build-up of the electron cloud is strongly dependent on the bunch separation, which scales with the damping ring circumference. Longer rings with larger bunch spacing are preferable to mitigate the development of the electron cloud.

The threshold for the fast head-tail instability can be found by applying the Keil-Schnell-Boussard criterion, which is based on a coasting beam model, and by approximating the electron-cloud effect as a broadband resonator impedance [21].

The analytic threshold cloud density for a given bunch intensity is given by [22 23]

$$\rho_{e,th} = \frac{2\gamma\nu_s\omega_e\sigma_z / c}{\sqrt{3}KQr_e\beta C} \qquad (2)$$

where β is the average vertical beta function, ν_s is the synchrotron tune, r_e is the classical electron radius, γ is the relativistic factor, σ_z is the bunch length, Q characterizes the quality-factor of the resonator and K is an enhancement factor due to the cloud size. The resonator frequency ω_e is given by the oscillation frequency of the electrons in the field of the beam, which in linear field approximation is given by

$$\omega_{e,y} = \sqrt{\frac{\lambda_+ r_e c^2}{\sigma_y(\sigma_x + \sigma_y)}} \qquad (3)$$

where λ_+ is the beam line density within the bunch and $\sigma_{x,y}$ are the transverse beam sizes. The coherent oscillation frequency in eq (3) is obtained by considering the electron cloud as a rigid Gaussian distribution with the same rms sizes as the beam.

The coasting beam model is appropriate if the electron phase advance $\omega_e\sigma_z/c$ related to the oscillation of the electron in the bunch potential is much larger than one, as is the case for all the reference lattices.

The analytical instability threshold values are summarized in Table 5. To apply equation (2) we use an approximate value of the beta function in the dipoles, the electron cloud in which is estimated to amount to the dominant contribution to the average electron density. For all the damping rings, the product of the effective broad-band resonator quality factor Q and the pinch parameter K was taken to be equal to $K \times Q = 3 \times 5$, the beta function $\beta = 30$ m (except for the TESLA ring, for which $\beta = 15$ m), and zero chromaticity [23]. In the table, the analytical estimates are compared with those given by simulation. The thresholds from the simulation are found to be systematically lower than

the thresholds expected from the analytical estimate. We suppose that the lower threshold density in the simulations is the result of the concentration and pinching of electrons under the influence of the attractive beam force. The force from the beam may be characterized by the electron phase advance during a bunch passage, $\omega_e\sigma_z/c$; a higher phase advance leads to a lower threshold density. In the B-factories, the phase advances are much smaller than in the damping rings, therefore the analytical estimates are in better agreement with the simulations. The instability threshold values found from the simulations are likely to be more reliable than those from the analytical estimates.

A smaller circumference, larger synchrotron tune and/or larger momentum compaction are helpful to mitigate the head-tail instability.

The critical issue is that the cloud build-up increases rapidly with short bunch spacing while the single-bunch instability has a much weaker and linear dependence on the ratio between the synchrotron tune and the circumference. Thus, a larger ring circumference is preferable.

Furthermore, the electron cloud can have a long-range memory that can drive coupled-bunch instabilities. The coupled-bunch growth times induced by the electron-cloud long-range wake field have been calculated[23] [24]using the PEI-M code. They are sufficiently long that a bunch-by-bunch feedback system can suppress the instability.

SIMULATION RESULTS

Different simulation codes have been benchmarked against each other with similar beam input parameters and secondary emission parameters. Nevertheless, differences in the secondary emission models exist and different codes include different features.

Typically, the electron cloud simulations are sensitive to the modeling of the secondary

emission process. As an example, a re-diffused electron component can be included in the secondary emission model[15] in code I. If the re-diffused component is included in the secondary emission model, the simulated cloud density may be, in some cases, larger[25] by a factor up to 2.

Electron cloud build-up

Figure 1 shows the simulated single-bunch instability thresholds together with the simulated central density obtained by build-up simulations, integrated over all the magnets and drift spaces for each of the eight lattices considered. Also, to set these values into perspective, the simulated cloud densities are indicated for peak secondary emission yields δ_{max}=1.2 and 1.4; the latter values are typical for those achieved in an accelerator environment after conditioning (electron and photon bombardment) of copper and stainless steel chambers or for chambers coated with thin films like TiN or TiZrV. Solenoid windings suppressing the electron cloud are assumed to be installed in all field-free regions.

Table 6 summarizes the results of simulations of electron cloud build-up in the positron damping rings, for a peak SEY of the chamber surface of 1.2. The value quoted for the density is the value reached at equilibrium after a number of bunch passages, averaged across a circular region of radius 1 mm centered at the beam. This central region may be compared with the beam sizes shown in Table 1. The arc and drift chambers are assumed to have a circular cross-section, with diameter depending on the region of the machine, as shown in Table 2.

It is not yet clear whether conditioning reduces the SEY below ~1.2 in an accelerator environment. Direct *in situ* measurements in the SPS showed that an electron cloud

activity decreased considerably with time and the SEY remained constant after a few days of scrubbing[26], with the δ_{max} value oscillating between 1.5 and 1.6. Notably, after short periods without beam scrubbing, the SEY drifted up from 1.5 to 1.7 in two week time. Further direct experimental measurements are ongoing to resolve this issue [27] [28] [29] [30] [31]. At present, it is considered a challenge to reduce in a stable way the SEY below 1.2 in accelerator vacuum chambers under operational conditions.

The SEY limits are tighter and the instability threshold is more likely to be exceeded in smaller rings. Note that for the MCH ring, simulations were performed with maximum available bunch spacing of 18.8 ns (rather than 15.4ns and train gaps).

We also considered the alternative configuration of two 6 km positron damping rings sharing the same tunnel; for simplicity we refer to this configuration as 2xOCS. This effectively provides a 12 km damping ring configuration with maximum bunch spacing of 14.4 ns, and considerably reduces the build-up of the electron cloud compared to the single 6 km ring.

Furthermore, a larger chamber aperture is beneficial in reducing the electron cloud build-up. In particular, we have simulated wiggler sections with different chamber apertures ranging from rectangular 32 mm x 18 mm aperture (original TESLA design) to larger round apertures of 32 mm up to 46 mm (CESR superconducting wiggler type) and the results for the 6 km and 12 km rings are shown in Fig. 2. In particular, in the 12 km ring with wiggler apertures larger than 32 mm, the initial seed of photoelectrons is dominating over the secondary emission process and statistical fluctuations of photoelectrons background in wigglers and arcs are visible between 32 mm and 46 mm apertures.

Wiggler and arc bend build-up simulations and codes benchmarking

We consider two wiggler-field models. The first model is a Cartesian representation of the wiggler field:

$$\begin{aligned} B_x &= 0 \\ B_y &= B_0 \cos(k_z z)\cosh(k_z y) \\ B_z &= -B_0 \sin(k_z z)\sinh(k_z y) \end{aligned} \qquad (4)$$

with $k_z = 2\pi/\lambda_w$, for wiggler period λ_w. Alternatively, we considered a cylindrical mode expansion valid for the TESLA wiggler[32], but the calculation of the wiggler field with the cylindrical model was very computer time intensive and we opted to use the Cartesian representation (4) for most of our simulations. Wiggler period and field are taken to be, respectively, λ_w =0.4 m, B_0=1.6 T.

Wiggler simulations for the OCS ring, using two different codes are shown in Fig. 3 and 4. Histograms of the cloud density in an OCS bend are shown in Fig. 5. Two stripes appear at near ±3mm from the vacuum chamber horizontal center axis. The codes are consistent. Fig. 6, 7 and 8 refer to simulations of an arc bend with three different codes. The agreement is within a factor 2-3. Note that for the simulations considered here, the central density is computed over a circular cross-section of radius 1 mm, centered on the beam. In this small area, fluctuations of the cloud density due to space charge have been observed in simulations of arc bends with beam dimensions of comparable size; see Table 1. In future comparisons, we will consider a larger and more stable central area. Summarizing the result of the build-up code comparison, the various simulations show a maximum factor 2-3 difference at the highest cloud density and ~ 10 % difference in the threshold secondary yield, which is satisfactory. A more detailed report on simulation benchmarking is in preparation. In particular, the build-up codes I, II, and III agree very

well in the prediction of an electron cloud that exceeds the instability threshold in a 6 km ring and of an electron cloud that is reduced and below the instability threshold in a ring of circumference 12 km or larger. This gives a good level of confidence in the codes' prediction capability.

Single-bunch instability simulations

Here, we show simulation results obtained from a strong-strong code[33], in which a bunch of positrons and the electron cloud are each represented by macroparticles, and the interactions between the beam and the cloud are applied at several, or several tens of positions around the ring, assuming a uniform beta function. Since the interaction points are discrete, an artificial incoherent emittance growth sometimes appears[34 35], from which the head-tail instability has to be distinguished. The head-tail instability appears with a sufficient number of interactions in a synchrotron period.

Furthermore, recent studies showed that there should be several interaction points per betatron wavelength, otherwise a significant incoherent emittance growth at densities far below the coherent instability threshold may appear in simulations [36 37].

To determine whether an observed emittance growth is the result of the fast head-tail instability, tests are carried out to see whether the emittance growth is independent of the number of interactions; if this is the case, then the emittance growth is indeed the result of the fast head-tail instability.

Figure 9 shows the emittance growth resulting from the fast head-tail instability caused by electron cloud for the damping ring lattices. Each plot shows the emittance growth for various cloud densities. The threshold density is determined by the density at which the

emittance growth first appears. The values indicated refer to the average cloud density around the ring.

Figure 10 shows a snapshot of the vertical centroid positions of the bunch and the cloud, and of the vertical beam size, as a function of the longitudinal position along the bunch. The cloud density is above threshold. The amplitudes of the coherent motion of the bunch and the cloud increase with the beam size, indicating that in this case the fast head-tail instability is the dominant cause of the emittance growth.

The instability threshold values are summarized in Table 5, and shown in Fig 1 and 2. The analytical estimates are compared with those given by simulation. The thresholds from simulation are systematically lower than the thresholds found from the analytical estimate.

FURTHER BUILD-UP SIMULATIONS AND CODE BENCHMARKING

Simulation codes have been benchmarked also with parameters different from the nominal beam parameters. In particular, simulations were carried out for different bunch spacings and chamber apertures.

In the following, we dedicate a paragraph to further simulations and code benchmarking.

TESLA wiggler code benchmarking

To benchmark the codes against each other, we have performed simulations with codes I and II, with primary photo-electron rate of 0.007 electrons per passing positron per meter taken for ECLOUD simulations of the TESLA wiggler[1]. Photo-electrons were uniformly emitted outside the antechamber slots. Elastic electron reflection was described by the Hilleret formula. Figure 11 shows the simulated build up of average electron cloud line density for the TESLA ring during the passage of two bunch trains with 72 bunches each

and a bunch-to-bunch gap of 8 missing bunches, using code II (Note that the inclusion of gaps is here artificial and it is only meant to reveal the cloud decay and rise times between successive bunch trains). Figure 12 shows simulation results for the TESLA ring using code I, with different values of δ_{max}. One may want to compare the simulation results obtained with the two codes when similar parameters are used, namely the case with photoelectron rate 0.007 e/p/m in Fig. 11 with the case of δ_{max}=1.3 in Fig. 12. These two cases agree to within 40%.

6 km and 12 km rings code benchmarking

We further benchmarked the codes for the 6-km OCS and the 12-km 2xOCS rings with beam and chamber parameters different from the nominal values of Table 1. Namely, we have used a larger bunch spacing of 7.2ns and an arc chamber with a larger diameter of 50mm. We compared the simulations results for an arc bend and for different SEY values obtained from codes I and II; see Figs. 13 and 14. The central density here is also computed within a larger region of radius 2.5mm (rather than 1mm used previously) centered on the beam. The agreement is within a factor 2.

Note that the central cloud density shown so far was computed within a region of radius 1 mm or 2.5 mm centered on the beam, respectively, corresponding to 1.5 or 4 times the average rms beam size in the OCS or 2xOCS arc cells (see Table 1). In arc bend simulations, a long-term variation of the central cloud density inside these small areas near the beam is often visible, for example, in Fig 15 for a SEY larger than 1.5. This variation is attributed to dynamic changes in the space-charge forces, occurring as the cloud evolves.

The average electron energy of electrons impinging on the chamber wall of the arc bends and straights for OCS and 2xOCS is displayed in Fig 16.

RECOMMENDATION

The advantages of a 6 km damping ring with a high degree of lattice symmetry are a significantly increased dynamic aperture, reduced space charge effects and improved machine availability and reliability with lower costs. However, shorter rings have a closer bunch spacing, which greatly enhances the build-up of the electron cloud. The electron cloud can be difficult to suppress in the dipole and wiggler regions where it is expected to be most severe, and the instabilities associated with the electron cloud could significantly affect the performance of the damping rings.

The KEKB and PEP-II B-factories have applied external solenoid fields to mitigate the electron cloud in field-free regions, which constitute a large fraction of those rings[38] [39].

The ILC damping rings typically do not have long field-free regions. Over most of the ring, the beam pipe is surrounded by magnets, such as wigglers and dipoles, where large electron cloud densities may develop. In magnetic field regions, external solenoid fields are not effective at suppressing the build-up of the electron cloud. It is worth noticing that the electron cloud effect in KEKB remains a major obstacle to shorter bunch spacing and higher luminosity, even with solenoid windings[40].

A large bunch spacing, therefore, is desirable to limit the build-up of the electron cloud. Also, a large synchrotron tune raises the threshold for the electron cloud driven instability.

The damping ring configuration option lattices may be listed in order of preference from the point of view of electron cloud, as (see Figure 1): MCH, TESLA, DAS, 2xOCS,

BRU, OCS. MCH and BRU are preferable in their respective circumference ranges because of their large synchrotron tune and/or momentum compaction.

As a general consideration, simulations show that in the ILC damping rings, larger chamber sizes are beneficial to reduce the electron cloud. In particular, increasing the wiggler full aperture beyond the nominal 18 mm assumed in these simulations further reduces the cloud density in the 2xOCS to a margin safely below the threshold for instability. With larger wiggler apertures, the 2xOCS ring can accommodate rather large values of SEY.

If the secondary electron yield can stably be reduced to δ_{max}=1.1 in the magnet regions then one single 6 km ring for the positrons may be feasible.

Based on the above considerations, the recommendation for the baseline configuration[23] was that the positron damping ring should consist of two (roughly circular) rings of approximately 6 km circumference in a single tunnel. Electron-cloud effects make a single ring of circumference 6 km or lower unattractive, unless significant progress can be made with mitigation techniques.

Possible cures in wiggler and dipole regions include grooves cut into the vacuum chamber, and the use of clearing electrodes[41 42 43 44]; see also Fig 4. Although very promising, these techniques need further studies and a full demonstration. Nevertheless, recent simulations indicate that proper mitigation techniques may possibly allow for a single 6-km circumference ring, a cost-saving option which presently is under scrutiny. Further news about electron cloud clearing techniques and simulations is expected from two future workshops[45 46].

AKNOWLEDGMENTS

We would like to thank to S. Guiducci, J. Gao and the contributors to the ILC damping rings configuration recommendation for their encouragement and helpful information. Many thanks also go to M. Furman, Y. Suetsugu, M. Jimenez, F. Le Pimpec, R. Kirby and N. Hilleret for very useful discussions.

LIST OF TABLES

Table 1. Parameters for possible ILC positron damping rings. Beam sizes are the calculated mean values in respective cells. Parameters used for build-up simulation.

Lattice	PPA	OTW	BRU	OCS	2×OCS	MCH	DAS	TESLA
Circumference [m]	2824	3223	6333	6114	12228	15935	17014	17000
Energy [GeV]	5.0	5.0	3.74	5.066	5.066	5.0	5.0	5.0
Harmonic Number	4700	7678	13732	13256	13256	34550	28377	28200
Bunch charge [10^{10}]	2.4	2.2	2.0	2.0	2.0	2.0	2.0	2.0
Bunch Spacing [ns]	4.0	4.2	6.154	6.154	14.4	15.38	20.0	20.12
Momentum compaction [10^{-4}]	2.83	3.62	11.9	1.62	1.62	4.09	1.14	1.22
Bunch length [mm]	6.0	6.0	9.0	6.0	6.0	9.0	6.0	6.0
Energy spread [10^{-3}]	1.27	1.36	0.97	1.29	1.29	1.3	1.3	1.29
Synchrotron Tune [10^{-2}]	2.69	4.18	12.0	3.37	3.37	15.0	6.6	7.1
Horiz. geometric emittance [nm]	0.43	0.39	0.37	0.55	0.55	0.67	0.61	0.5
Vertic. Geometric emittance	2.0	2.0	2.0	2.0	2.0	1.4	1.4	1.4
Mean horiz. β function [m]	13.1	58	57.6	25.6	25.6	109	106	120
Mean vert. β function [m]	12.5	63.8	55	31	31	108	106	121
Hor. Beam size in arc cell [um]	370	370	620	620	620	360	360	360
Ver. Beam size in arc cell [um]	7	7	8	8	8	6	6	6
Hor. Beam size straight cell [um]	180	180	130	130	130	240	240	240
Ver. Beam size straight cell [um]	13	13	9	9	9	14	14	14
Hor. Beam size wiggler cell [um]	40	40	93	93	93	90	90	90
Ver. Beam size wiggler cell [um]	3	3	4.2	4.2	4.2	5.6	5.6	5.6

Table 2. Baseline vacuum chamber aperture (diameter) in different regions of the ILC damping rings, used for simulations of the electron cloud build-up.

DR Region	Chamber aperture [mm]
Long Straight	100
Arc Drift	44
Bend	44
Quadrupole	44
Sextupole	44
Antechamber in arc, full aperture	10
Wiggler rectangular aperture (TESLA)	32 x 18
Wiggler larger round aperture	32
Wiggler larger round aperture (CESR)	46
Antechambers (2) in wiggler full aperture	6

Table 3. Set of simulation parameters used for the electron cloud build-up simulations presented in this paper. Primary photoelectron rate. Units are photo-electrons per meter per beam particle.

Lattice	BRU	OCS	2×OCS	MCH	DAS	TESLA	PEP	KEK
Arc photoelectron rate [e-/m/e+]	0.0014	0.0014	0.0014	0.0014	0.0014	0.0014	3e-4	3e-4
Wiggler photoelec rate [e-/m/e+]	0.007	0.007	0.007	0.007	0.007	0.007	-	-
Straight photoelec rate [e-/m/e+]	-	-	-	0.0014	0.0014	0.0014	3e-4	3e-4
Photon reflectivity [%]	80							

Table 4. Beam parameters used for B-factories build-up simulation.

Lattice	PEP-II LER	KEKB LER
Circumference [m]	2199	3016
Energy [GeV]	3.1	3.5
Bunch charge [10^{10}]	9	3.3
Bunch Spacing [ns]	4.2	6
Bunch length [mm]	12.5	4
Hor. Beam size in arc cell [um]	700	424
Ver. Beam size in arc cell [um]	230	60
Hor. Beam size straight cell [um]	700	424
Ver. Beam size straight cell [um]	230	60

Table 5. Analytical and simulated threshold densities for fast head-tail instability driven by electron cloud, and parameters assumed for the estimation. The density thresholds refer to the values of the average cloud density over the ring.

	PPA	**OTW**	**OCS**	**BRU**	**MCH**	**DAS**	**TESLA**	**PEP-II**	**KEK-B**
γ	9785	9785	9914	7319	9785	9785	9785	6067	6849
ν_s	0.027	0.042	0.034	0.12	0.15	0.06	0.071	0.030	0.015
$\omega_e\sigma_z/c$	15	15	15	15	15	15	15	3	3
KQ	15	15	15	15	15	15	15	9	9
β [m]	30	30	30	30	30	30	15	18	11
ρ_e,th [mm^{-3}]	1278	1742	753	1894	1258	526	1116	628	425
ρ_e,sim [mm^{-3}]	-	400	140	300	300	120	240	--	400

Table 6. Electron cloud density in different sections of the positron damping rings. The chamber peak SEY is 1.2, and there is no solenoid in the drift sections.

		OCS	BRU	2×OCS	MCH	DAS	TESLA
Long Straight	Length [m]	0	0	0	11761	13214	14242
	ρ_e [mm^{-3}]	0	0	0	2	2	2
Arc Drift	Length [m]	5211	4092	5211	1876	2368	1345
	ρ_e [mm^{-3}]	300	194	79	40	40	40
Dipole	Length [m]	434	1445	434	1445	654	695
	ρ_e [mm^{-3}]	400	400	39	28	28	28
Quadrupole	Length [m]	178	254	178	311	323	200
	ρ_e [mm^{-3}]	300	300	21	8	8	8
Sextupole	Length [m]	96	101	96	101	22	100
	ρ_e [mm^{-3}]	300	300	21	8	8	8
Wiggler	Length [m]	196	441	196	441	433	417
	ρ_e [mm^{-3}]	9200	9200	1200	650	650	650
Total	Length [m]	6114	6334	6114	15935	17014	17000
	ρ_e [mm^{-3}]	592	943	110	27	25	22

LIST OF FIGURES

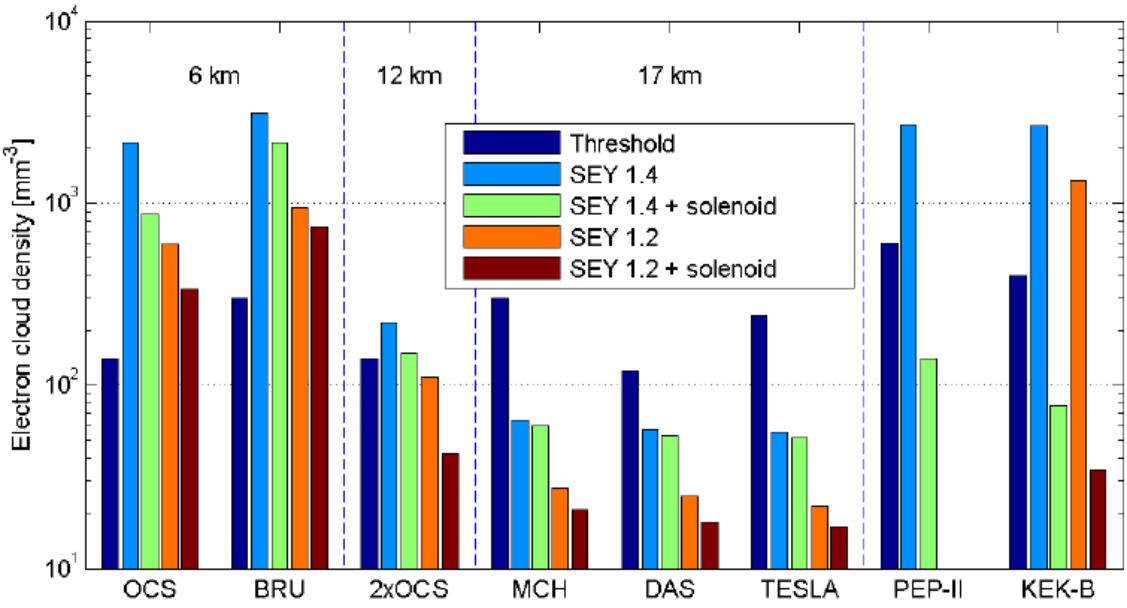

Figure 1: Instability thresholds and average *central* cloud densities for various SEY and solenoid combinations in the different damping ring configurations and the B factories. A wiggler vertical full aperture of 18mm is assumed in these simulations. Solenoid windings are assumed to be arranged in field free regions. Using code I and IV.

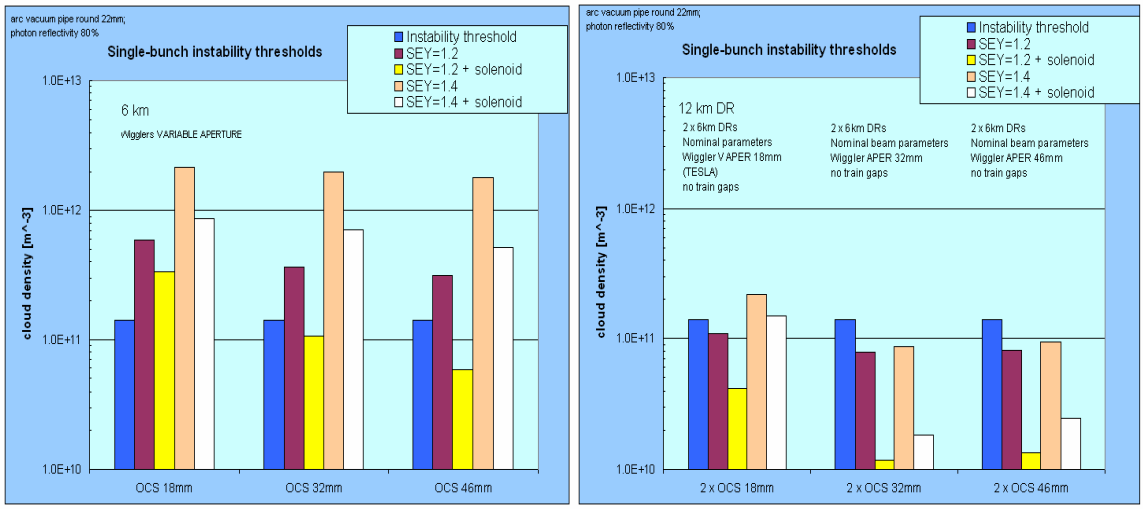

Figure 2: Beneficial effect of increasing the wiggler chamber aperture in the 6 km ring (Left) and 12 km ring (Right). Average *central* cloud density over the ring for various SEY and solenoid combinations assuming 18, 32 and 46 mm wiggler apertures. In particular, in the 12 km ring with wiggler apertures larger than 32 mm, the initial seed of photoelectrons is dominating over the secondary emission process and statistical variation of the photoelectrons background in wigglers and arcs explains small differences seen between the 32-mm and 46-mm apertures. Using code I and IV.

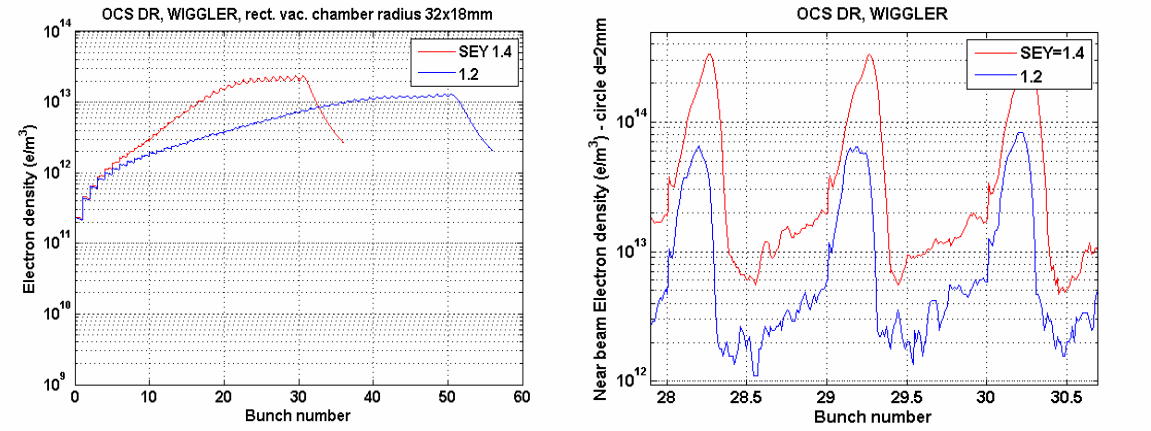

Figure 3. Simulated electron cloud density in a wiggler section of OCS; using code I. A rectangular cross section of width 32 mm and height 18 mm is assumed. Results are shown for SEY 1.4 (upper curve) and 1.2 (lower curve).

(Left Figure) The electron cloud density is averaged over the cross section of the chamber. (Right figure) The central cloud density is shown. The central density is averaged over a circular cross-section of radius 1 mm, centered on the beam. The central cloud density just before a bunch passage is found at integer values of the bunch number.

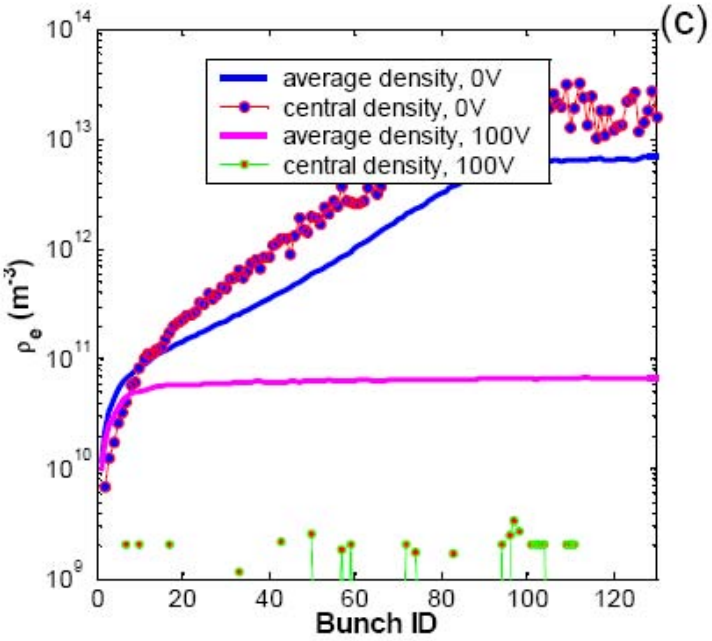

Figure 4: Electron cloud density in a wiggler in OCS assuming SEY 1.74. The values densities shown are the central density just before the bunch passage (upper curve) and the average chamber density (second from top curve). Clearing electrodes have also been used for this simulation. Code III.

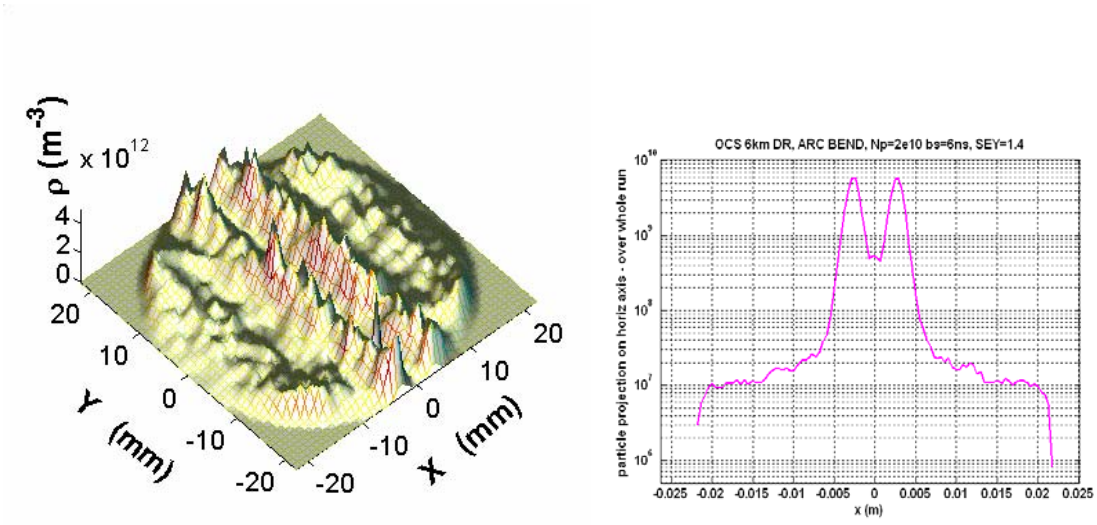

Figure 5: Histograms of the electron cloud in an arc bend in OCS with two different simulation codes: using (Left) code III and (Right) code I. Two vertical stripes appear near the central region of the chamber. The left plot shows the 2D histogram of the cloud density. The right plot shows the projection onto the horizontal axis (a.u.) of the particles accumulated over the whole run.

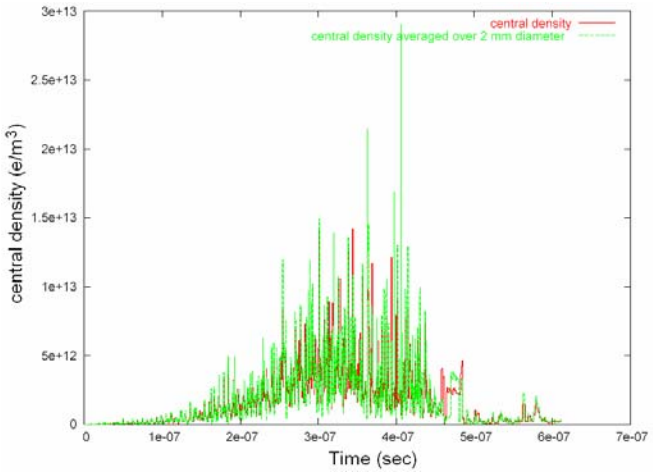

Figure 6: Code II. Electron cloud central density in an arc bend of the OCS ring, with circular vacuum chamber of radius 22 mm and SEY 1.4. The plot shows the central density and the density averaged over a circular cross-section of radius 1

mm, centered on the beam. The pinching effect is visible by the enhancement of the central density during one bunch passage.

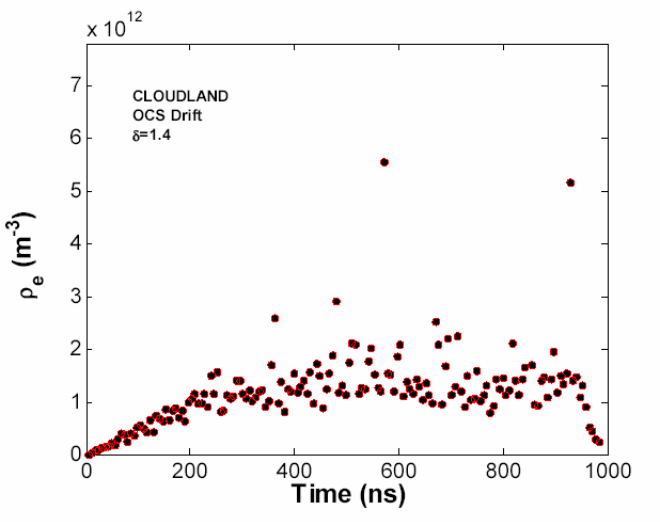

Figure 7: Code III. Electron cloud density in an arc bend of the OCS ring, with circular vacuum chamber of radius 22 mm and SEY 1.4. The plot shows the central density just before the bunch passage, averaged over a circular cross-section of radius 1 mm and centered on the beam.

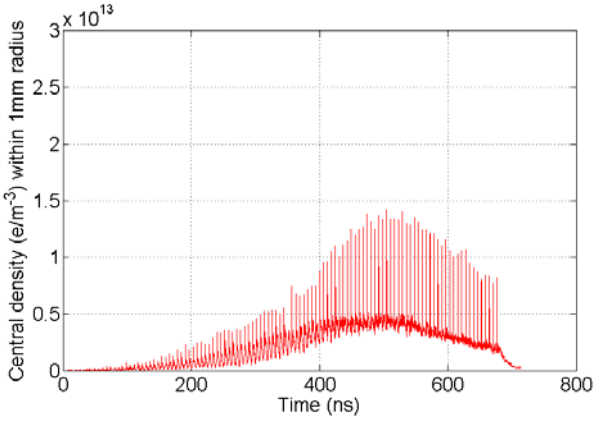

Figure 8: Code I. Electron cloud central density in an arc bend of the OCS ring, with circular vacuum chamber of radius 22 mm and SEY 1.4. The plot shows the cloud density averaged over a circular cross-section of radius 1 mm, centered on the

beam. The pinching effect is visible by the enhancement of the central density during bunches passage.

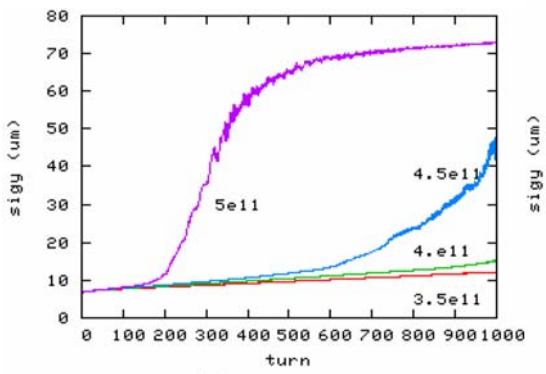

(a) OTW

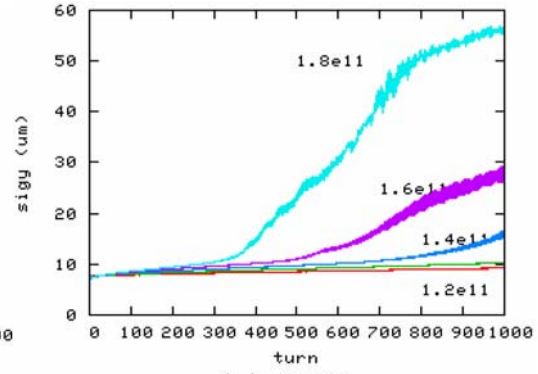

(b) OCS

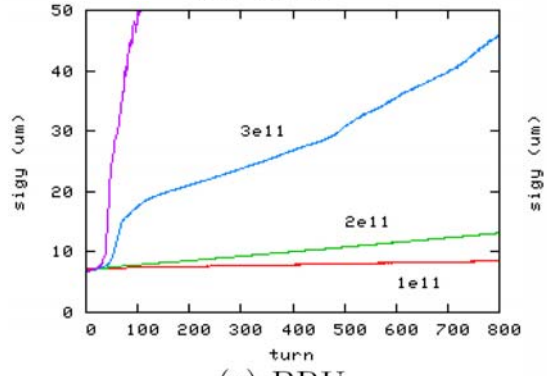

(c) BRU

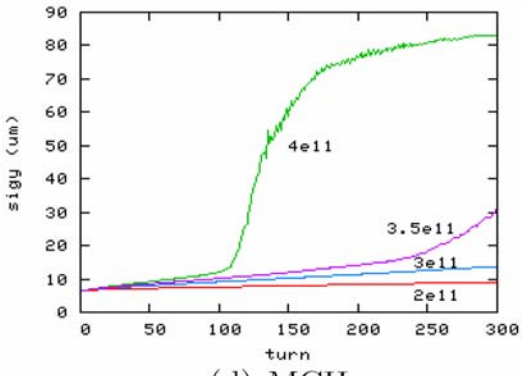

(d) MCH

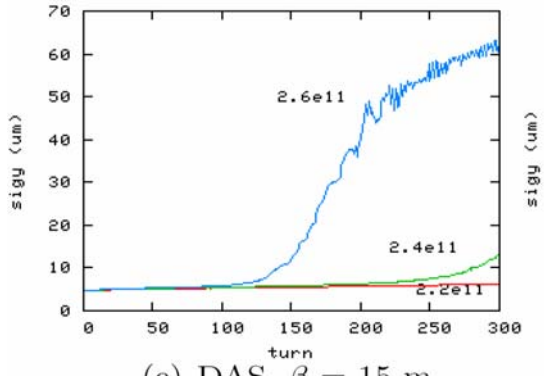

(e) DAS, $\beta = 15$ m

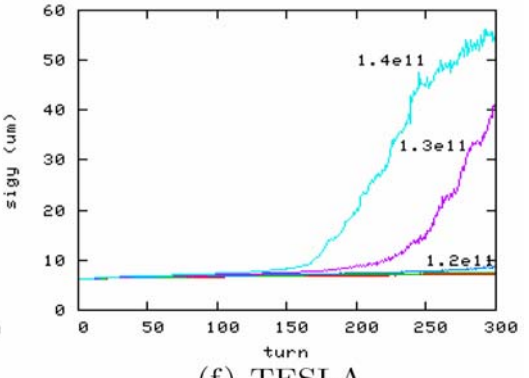

(f) TESLA

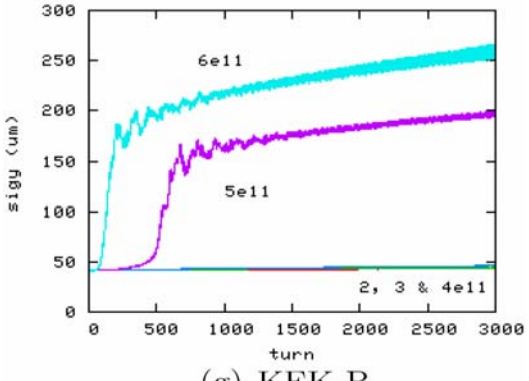

(g) KEK-B

Figure 9: Emittance growth from single-bunch instability driven by electron cloud. Using code IV.

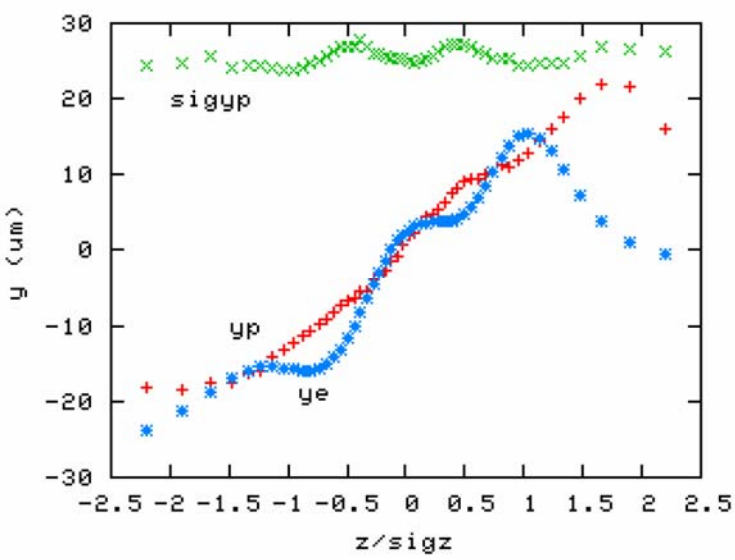

Figure 10: Beam and electron cloud profiles along a bunch in OCS after 1000 turns, with $\rho_e = 1.6 \times 10^{11}$ m^{-3}. The bunch size and the centroids of the bunch and electron cloud are shown. Using code IV.

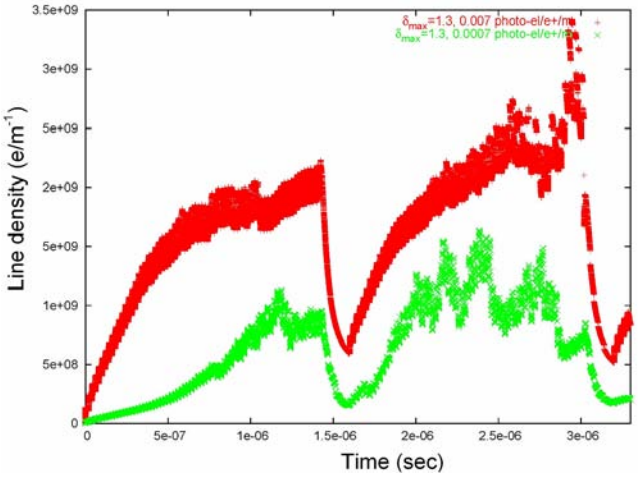

Figure 11. Simulated electron line density in a TESLA wiggler section as a function of time, using δ_{max}=1.3 and a primary photoelectron rate of either 0.007 or 0.0007 electrons per meter and per beam positron. Hilleret model[13] for e- reflection is used in this simulation: using code II.

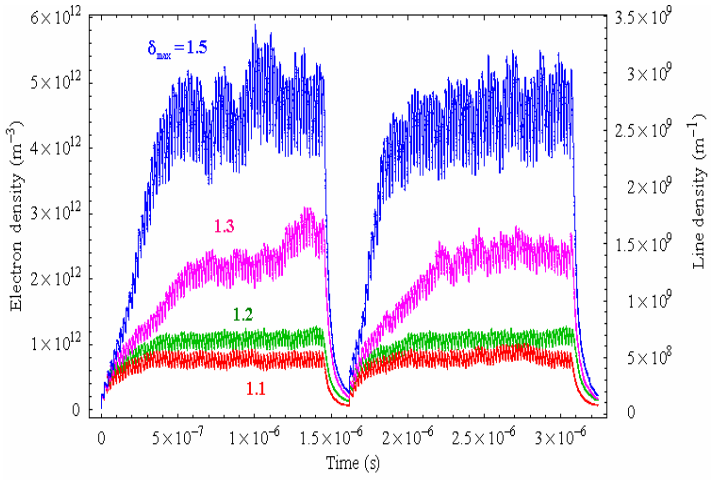

Figure 12. Simulated electron density averaged over the chamber for the TESLA ring, using different values of δ_{max} 1.1, 1.2, 1.3 and 1.5, and a primary photoelectron rate of 0.007 electrons per meter and per beam positron: using code I. Note that the cloud density is shown in units of e/m^3 or e/m respectively on the left and right axis.

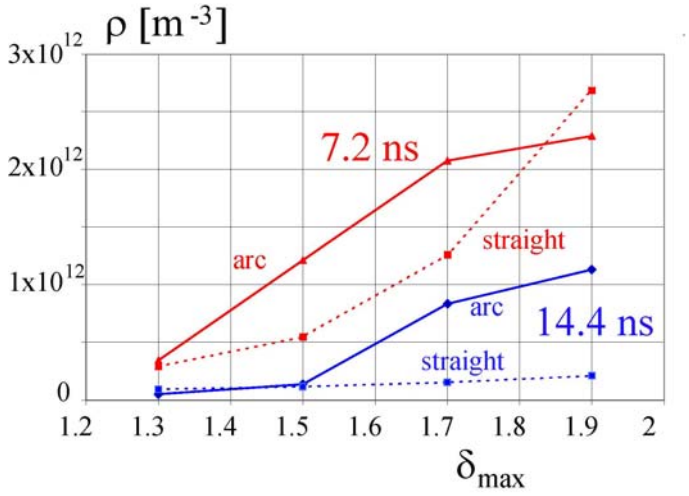

Fig 13. Central cloud density as a function of the peak secondary electron yield in arc bend and straight sections, for a bunch spacing of 7.2 ns and 14.4 ns and a chamber aperture of 50mm. The central density is computed in an area 2.5mm radius centered at the beam: using code II.

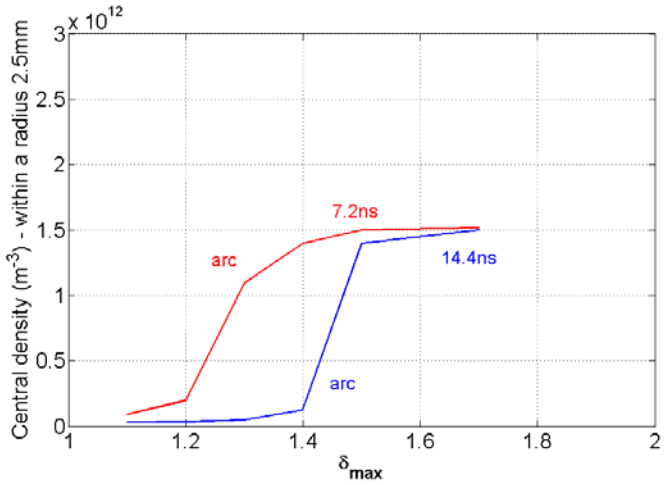

Fig. 14. Central cloud density as a function of the peak secondary electron yield value in arc bend, assuming bunch spacing of 7.2 ns and 14.4 ns and an arc chamber aperture of 50mm. The central density is computed in an area 2.5mm radius centered at the beam: using code I.

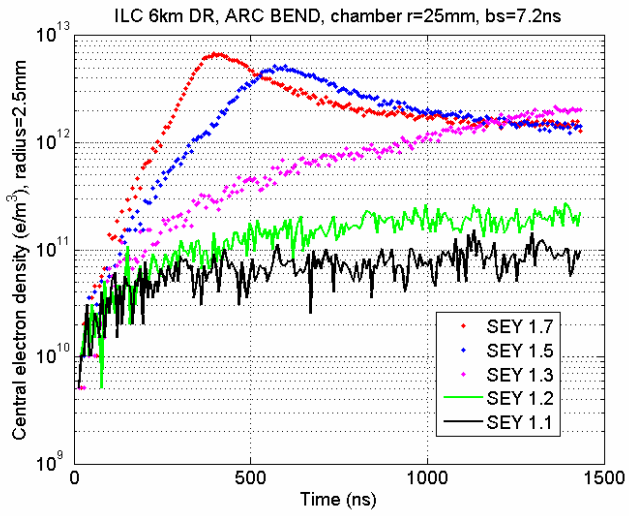

Fig. 15. Central cloud density plotted just before the bunch passage, for a bunch spacing of 7.2ns for an arc bend of the OCS ring and chamber aperture 50mm. The cloud density is computed in an area of 2.5 mm radius centered at the beam, using code I.

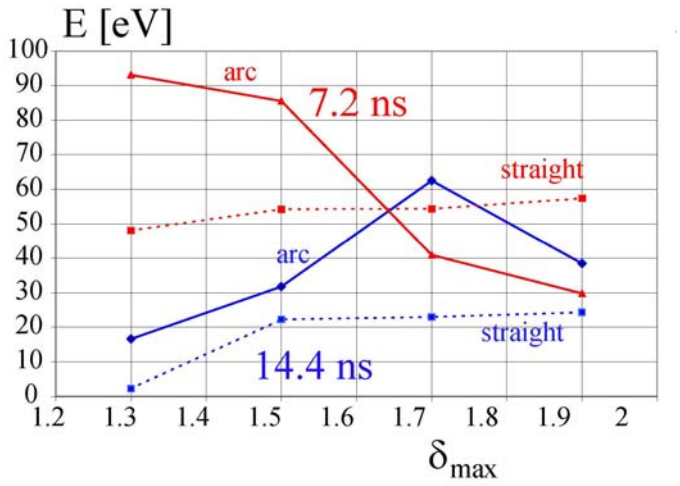

Fig 16. Average electron energy for electron impinging at the wall, using code II.

---

[1] K. Ohmi, M. Pivi, G. Rumolo, D. Schulte, R. Wanzenberg and F. Zimmermann contributions in *Proceeding of the ECLOUD04 Workshop*, Napa, CA, USA (2004) and PAC05 Conference, Knoxville, TN, USA (2005).

[2] Electron cloud in the LHC http://ab-abp-rlc.web.cern.ch/ab-abp-rlc-ecloud/

[3] K. Ohmi, Phys. Rev. Lett. **75**, 1526 (1995).

[4] H. Fukuma et al., in the *Proceedings* of EPAC 2000 Conference, Vienna, Austria.

[5] G. Arduini, K. Cornelis, W. Hoefle, G. Rumolo, F. Zimmermann, in the *Proceedings* of PAC 2001, Chicago and CERN-SL-2001-0050.

[6] D Schulte, G. Arduini, V. Baglin, J.M. Jimenez, F. Ruggiero, F. Zimmermann , *Electron Cloud Measurements in the SPS in 2004*, in the Proceedings PAC2005 Knoxville, LHC Project Report 847.

[7] A. Kulikov, A. Fisher, S. Heifets, J. Seeman, M. Sullivan, U. Wienands, W. Kozanecki, in the *Proceedings* PAC-2001 Chicago, Illinois U.S.A. edited by P. Lucas, S. Webber.

[8] A. Kulikov, A. Novokhatski, J. Seeman SLAC-PUB-10886, Dec 2004.

[9] K. Oide, prepared for 11th Workshop on LEP Performance, Chamonix, France, 2001.

[10] Q. Qin, Z.Y. Guo, H. Huang, Y.D. Liu, J. Xing, J.Q. Wang, Z. Zhao Nucl. Instrum. Meth. A547, 239-248,2005.

[11] J. Wei, M. Blaskiewicz, W. Fischer, H.C. Hseuh, U. Iriso, T. Roser, L. Wang, S.Y. prepared for HHH-APD Workshop, Geneva, Switzerland, 8-11 Nov 2004.

[12] http://www-project.slac.stanford.edu/ilc/testfac/ecloud/elec_cloud_comparison.html

[13] N. Hilleret et al., ECLOUD'02 Proceedings, CERN-2002-001 (2002).

[14] R. Kirby and F. King, Nucl.Instrum.Meth. **A469**, 1-12 (2001).

[15] M.A. Furman and M.T.F. Pivi Phys.Rev.ST Accel.Beams **5** 124404, (2002).

[16] R. Cimino, I.R. Collins, M.A. Furman, M. Pivi, F. Ruggiero, G. Rumolo, F. Zimmermann Phys. Rev. Lett. **93**, 014801,2004.

[17] F. Zimmermann *et al.*, in Proceedings EPAC06 Conference, Scotland, (2006).

[18] F. Ruggiero, F. Zimmermann, Simulation Codes Web Repository http://care-hhh.web.cern.ch/care-hhh/simulation_codes_catalogue_and_repository.htm

[19] K. Ohmi and F. Zimmermann, Phys. Rev. Lett. 85, 3821 (2000).

[20] G. Rumolo et al, in the *Proceedings* of PAC 01, Chicago, Illinois (2001).

[21] K. Ohmi, F. Zimmermann, and E. Perevedentsev, Phys. Rev. E **65** , 016502 (2002).

[22] K. Ohmi, Proceedings of ECLOUD04, Napa, California, (2004).

[23] A. Wolski, J. Gao, and S. Guiducci, LBNL–59449 (2006).

[24] https://care-hhh.web.cern.ch/care-hhh/Simulation-Codes/References%20pages/Ref_PEI-M.htm

[25] M. Furman and M. Pivi LBNL private communication (2002).

[26] M. Jimenez, G. Arduini, V. Baglin, P. Collier, G. Ferioli, B. Henrist, N. Hilleret, L. Jensen, B. Jenninger, J.M. Laurent, A. Rossi, K. Weiss, F. Zimmermann, "*Electron Clouds – Results From SPS and Experiments For 2003"* in the *Proceedings* of Chamonix XII Workshop, France, (2003) http://ab-div.web.cern.ch/ab-div/Conferences/Chamonix/chamx2003/PAPERS/10_1_JJM.pdf

[27] Y. Suetsugu, K. Kanazawa, K. Shibata and H. Hisamatsu Nucl. Instrum. Methods Phys. Res. A **556,** Issue 2**,** 399-409 (2006).

[28] Y. Suetsugu et al., Nucl. Instrum. Meth. **A554**, 92-113, (2005).

[29] F. Le Pimpec et al., Nucl.Instrum.Meth. **A551**, 187-199 (2005).

[30] M. Pivi, F. Le Pimpec, R. Kirby, and T. Raubenheimer, in *Proceedings of PAC05 Conference*, Knoxville, TN, USA, (2005).

[31] F. Le Pimpec et al., SLAC-TN-04-046.

[32] M. Woodley and A. Wolski, LBNL, CBP-Tech Note-276 pg. 14.

[33] K. Ohmi in the *Proceedings* of PAC 2001, Chicago, Illinois (2001).

[34] E. Benedetto et al., in the *Proceedings* of PAC 2005, Knoxville, Tennessee (2005).

[35] K. Ohmi et. al., Phys. Rev. ST-AB **7**, 104401 (2004).

[36] E. Benedetto, G. Franchetti, F. Zimmermann, Incoherent effects of electron clouds in proton storage rings, Phys.Rev.Lett.97:034801 (2006).

[37] K. Ohmi (Memo), 19 November 2002, http://wwwslap.cern.ch/collective/ecloud02/ecsim/ecirb.pdf

[38] H. Fukuma, "Electron Cloud Effects in KEK-B," in the *Proceedings* of ECLOUD'04, Napa, California (2004) and CERN-2005-001.

[39] A. Kulikov, A. Novokhatski and J. Seeman, "Suppression of the Beam Instability Related to Electron Cloud at PEP-II B-Factory," in the *Proceedings* of ECLOUD'04, Napa, California (2004). CERN-2005-001.

[40] KEKB 2005 Annual Report, p.2, http://www-kekb.kek.jp:16080/pukiwiki/index.php?Documents

[41] L. Wang, G. Stupakov, T. Raubenheimer, MOPLS143, in *Proceedings EPAC06*. Also as SLAC-PUB-12001.

[42] L. Wang, H. Fukuma, S. Kurokawa, M. Pivi, and G. Xia, in *Proceedings EPAC06 Conference*, Edinburgh, Scotland, (2006).

[43] N. Diaczenko, A. Jaisle, P. McIntyre, and N. Pogue, report http://ab-abp-rlc.web.cern.ch /ab%2Dabp%2Drlc%2Decloud

[44] M. Pivi, R. Kirby, G. Stupakov, R. Kirby, F. King and F. Le Pimpec to be submitted to Phys. Rev. Lett. (2006)

[45] ECL2 Workshop on Electron Cloud Clearing, CERN Switzerland, February, (2007) http://care-hhh.web.cern.ch/care-hhh/ECL2/default.html

[46] ECLOUD07 Workshop, Kyungpook University, Daegu, South Korea, April, (2007).